Superelastic softening in perovskites

W. Schranz*

University of Vienna, Faculty of Physics, Physics of Functional Materials, Boltzmanngasse 5, A-1090 Wien, Austria

(Received 2 December 2010; published 25 March 2011)

Contrary to high frequency (MHz-GHz) elastic data, at low frequencies (0.1–50 Hz) huge elastic softening (*superelasticity*) is usually found in the low symmetry improper ferroelastic phases (i.e., tetragonal or rhombohedral) of perovskite structured materials including $SrTiO_3$, $KMn_{1-x}Ca_xF_3$, and $LaAlO_3$. This giant elastic softening is caused by domain wall motion and can be suppressed with uniaxial stress. Taking into account the long range interaction of needle shaped domains and the repulsion between domain walls of finite thickness a free energy is constructed. The temperature variation of the elastic susceptibility is calculated which yields perfect fitting of the data. Within this soliton model we can also describe the measured effect of applied stress.

DOI: 10.1103/PhysRevB.83.094120 PACS number(s): 62.20.−x, 62.40.+i, 61.72.Mm, 68.35.Ja

I. INTRODUCTION

Domain walls can contribute substantially to macroscopic properties of materials. One of the earliest experiments showed the influence of domain wall motion on the dielectric permittivity of ferroelectric KH_2PO_4.[1] In subsequent years the dynamical behavior of domain walls in ferroelectric materials was extensively studied, e.g., in $BaTiO_3$,[2] KH_2PO_4,[3–6] KH_2AsO_4,[7] and TGS.[8] Domain wall motion also contributes largely to the electromechanical response in ferroelectric ceramics such as $Pb(Zr,Ti)O_3$.[9] Nanodomains clearly play a key role in disordered ferroic materials[10] and even in strain glasses.[11] An excellent overview on domains and their properties is presented in the recent book of Tagantsev, Cross, and Fousek.[12] The problem of domains and domain wall motion is also well addressed in a review by Wadhawan.[13]

Theoretical calculations describing the influence of domain wall motion on the corresponding dynamic macroscopic susceptibilities exist mainly for ferroelectric[14–16] and ferromagnetic[17,18] materials. This is because in these systems an equilibrium free energy can be constructed, since a regular domain pattern is stable below T_c due to the competition between the domain wall energy and the long range depolarization[19] or demagnetization field, respectively. In ferroelastic crystals no analogous field exists, and as a result ferroelastic domains are in general metastable. Nevertheless, as many experiments have shown, ferroelastic domains appear as a rule below a ferroelastic phase transition[20,21] forming rather long lived objects. Due to mechanical compatibility[22] between adjacent domains they usually form well oriented stripes. Very often needle or dagger shaped domains[21,23–25] appear as will be discussed in detail below.

In recent years we have performed elastic measurements in quite a number of perovskite structured materials. Perovskites (ABX_3) display a wide variety of physical properties such as superconductivity, magnetism, ferroelectricity, and magnetoelectricity which make them very interesting for applications. But also in the geological context, the elastic and seismic properties of minerals with perovskite structure are important; e.g., in the deep earth mantle domain wall motion may influence their low frequency elastic and anelastic behavior at seismic frequencies.

Here we review the experimental situation concerning the low frequency elastic response of perovskites and present a model to describe the influence of ferroelastic domain wall motion to the low frequency elastic susceptibility of proper or improper ferroelastic materials. Applying it to the wealth of data on perovskite materials, i.e., on $SrTiO_3$,[26,27] $KMn_{1-x}Ca_xF_3$,[28] and $LaAlO_3$,[29] we show that the present model describes the observed superelastic softening perfectly as a function of temperature and applied stress.

II. PHASE TRANSITIONS IN PEROVSKITES

The parent phase of the studied crystals has the cubic perovskite structure with space group O_h^1 ($Pm\bar{3}m$). The phase transition of $SrTiO_3$ at $T_c = 105$ K as well as the high temperature phase transition in pure $KMnF_3$ at $T_{c1} = 186.5$ K are accompanied by a symmetry reduction $Pm\bar{3}m \rightarrow I4/mcm$. The phase transition in $LaAlO_3$ at $T_c = 813$ K leads to a reduction of symmetry from the cubic space group $Pm\bar{3}m$ to the rhombohedral subgroup $R\bar{3}c$.[30] All phase transitions are driven by rotations of BX_6 octahedra, where adjacent octahedra rotate in opposite senses, leading to a doubling of the unit cell. For $SrTiO_3$ and $KMnF_3$ the octahedra rotate around one of three equivalent $\langle 001 \rangle$ directions of the cubic phase, whereas for $LaAlO_3$ the rotation occurs around one of the four $\langle 111 \rangle$ directions. Due to the coupling between the primary order parameter and the strain components (square of the order parameter, linear in strain), the phase transitions in these systems are improper ferroelastic.[31]

Detailed calorimetric measurements have shown that the phase transitions in $SrTiO_3$[32] and $LaAlO_3$[33] are of second order, whereas the phase transition in pure $KMnF_3$[34] is weakly first order and close to a tricritical point. Substitution of Ca for Mn causes the transition to change from first to second order via a tricritical point at ≈0.3 mol % Ca.[35]

III. MEASUREMENT TECHNIQUE

For the low frequency elastic measurements a dynamical mechanical analyzer (DMA7, Perkin Elmer) was used. The samples are exposed to a given static force F_{stat} which is modulated by a dynamic force F_{dyn} of chosen amplitude and frequency ($f = 0.1$–50 Hz). The force can be tuned between 1 mN and 2.5 N. The amplitude u and the phase shift δ of the resulting elastic response of a sample are registered via inductive coupling with a resolution of $\Delta u \approx 10$ nm and

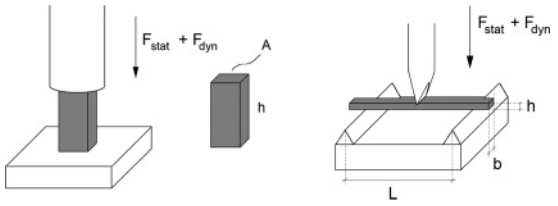

FIG. 1. Sketch of the measurement geometries for parallel plate (PPS, left) and three point bending (TPB, right).

$\Delta\delta \approx 0.1^\circ$. The knowledge of δ and u allows the determination of both real and imaginary parts of the complex Young's modulus $Y^* = Y' + iY''$, where $Y' = |Y^*|\cos\delta$ and $Y'' = |Y^*|\sin\delta$, and $\tan\delta = Y''/Y'$ measures the energy dissipation. Measurements have been performed by a parallel-plate stress (PPS) or three-point-bending (TPB) method (Fig. 1). For PPS geometry

$$Y^*(\mathbf{p}) = \frac{F_{\rm dyn}}{u}\frac{h}{A}\exp(i\delta), \tag{1}$$

where h and A represent the sample thickness and area, respectively, and $F_{\rm dyn}$ is the magnitude of the applied dynamic force in the $\mathbf{p}$ direction. In our PPS measurements we used samples with typical dimensions $A \approx 1$ mm^2 and $h \approx$ 3–5 mm.

For TPB one obtains

$$Y^*(\mathbf{q}) \approx \frac{F_{\rm dyn}}{u}\frac{L^3}{4bh^3}\exp(i\delta), \tag{2}$$

where L is the spacing between two bottom knife edges, typically 5 mm, h is the thickness of the sample, and b is the width of the sample. Here $\mathbf{q}$ points along the long axes of the sample bar, i.e., perpendicular to the direction $\mathbf{p}$ of the applied force. Typical sample thicknesses varied between 0.1 and 0.5 mm and $b = 2$ mm.

Equation (2) is an approximation; i.e., the complete formula contains also the inverse shear modulus[36] $G(\mathbf{p},\mathbf{q})^{-1}$. But since this term is multiplied by $(h/L)^2 \approx 10^{-4}$ its contribution can be neglected in the present study. There are however cases where this part dominates the elastic behavior in TPB geometry: Approaching a *proper* ferroelastic transition the shear modulus $G \to 0$ and therefore the part containing the inverse shear modulus overcomes the longitudinal contribution, making TPB a very convenient method to measure ferroelastic softening. We have previously applied this technique to study the influence of discommensurations near the lock-in transition of the incommensurate ferroelastic crystal $[N(CH_3)_4]_2CuCl_4$[36], yielding a Curie-Weiss type anomaly of the elastic susceptibility.

The absolute accuracy of DMA measurements is usually not better than 20%, whereas the relative accuracy is within 0.2%–1%. For more details on the method and its application to the investigation of phase transitions see also Refs. 37 and 38.

IV. MODELING THE DOMAIN WALL CONTRIBUTION TO THE ELASTIC COMPLIANCE

The elastic behavior of $SrTiO_3$, $KMnF_3$, $KMn_{1-x}Ca_xF_3$, and $LaAlO_3$ crystals measured in the Hz region differs in their ferroelastic phases drastically from the ultrasonic properties measured at MHz frequencies. The high frequency elastic response of these perovskite crystals is well described by Landau theory[27,28,39] whereas their low frequency elastic behavior below T_c is dominated by domain wall motion.

The influence of domain wall motion on macroscopic elastic[29,40–42] and dielectric properties[5,8,43,44] of materials is a rather complex mesoscopic problem which involves many length scales. It is a matter of active experimental and theoretical research[45] and is far from being completely understood. Nevertheless, as we shall see below, the experimental situation in perovskites is rather clear and the data can be well described in terms of a relatively simple model.

The symmetry reduction $Pm\bar{3}m \to I4/mcm$ which belongs to the ferroic species $m\bar{3}mF4/mmm$ leads to three possible domain states, say, O_1, O_2, O_3, where the spontaneous strains $\boldsymbol{\epsilon}_s(O_i)$ are in Voight notation given as[46]

$$\begin{aligned}\boldsymbol{\epsilon}_s(O_1) &= (\epsilon_s,\epsilon_s,-2\epsilon_s,0,0,0),\\ \boldsymbol{\epsilon}_s(O_2) &= (-2\epsilon_s,\epsilon_s,\epsilon_s,0,0,0),\\ \boldsymbol{\epsilon}_s(O_3) &= (\epsilon_s,-2\epsilon_s,\epsilon_s,0,0,0).\end{aligned} \tag{3}$$

Here $\epsilon_s = \sqrt{\frac{2}{3}}(e_1 - e_3) = \sqrt{\frac{1}{3}}\frac{a-c}{a_0} < 0$ since $c > a$ in the whole tetragonal phase of $SrTiO_3$[47] and $KMnF_3$.[48] The permissible orientations of domain walls can be calculated using Sapriel's approach[22] with the solutions $x = \pm z$ for O_1/O_2, $y = \pm z$ for O_1/O_3, and $x = \pm y$ for O_2/O_3. To calculate the domain wall contribution to the elastic susceptibility we use a simplified configuration of the domain structure containing only two types of domains, e.g., in the O_1 and O_2 states.

For $LaAlO_3$ the symmetry reduction $Pm\bar{3}m \to R\bar{3}c$ leads to four domain states with 12 nonequivalent twin orientations of the form $\{100\}$ and $\{110\}$.[29,33] The spontaneous strain components in this case are ϵ_1 and ϵ_4, corresponding to nonsymmetry breaking and symmetry breaking strains, respectively.[49]

To calculate the macroscopic elastic response of a multidomain crystal one has to calculate the corresponding effective spring constant for an array of ferroelastic twins from the corresponding free energy expression. However, unlike ferroelectric or ferromagnetic domains the ferroelastic domains are generally speaking metastable objects. Moreover, in contrast to the statements of some other works,[5,8] for perfectly planar ferroelastic domain walls of zero thickness which intersect the crystal completely, there is no elastic interaction which is sufficiently strong to matter in these considerations. As a result one cannot deduce an equilibrium configuration of ferroelastic domains for this case. However, there are several possible reasons for the appearance of ferroelastic domains below T_c. For specific boundary conditions Roytburd[50,51] has shown that the crystals can break into ferroelastic domains to reduce elastic energy at the phase front of a first order phase transition and that dynamical restoring forces exist. They will however vanish when the crystals leave the phase coexistence region.

At second order phase transitions the situation is quite different. There exists no long range elastic field and the domains simply appear for statistical reasons. If we envisage the domain wall energy which close to a second order phase transition scales as[21] $E_w \propto (T_c - T)^{3/2}$ as the activation

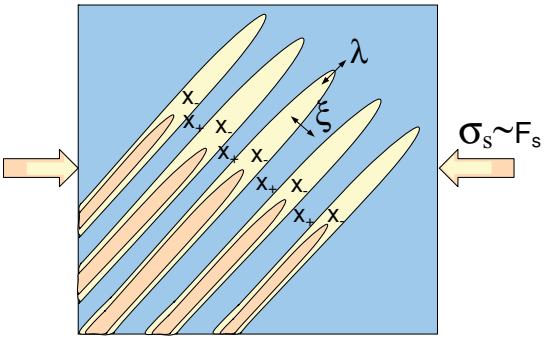

FIG. 2. (Color online) Sketch of needle domains of length l and width x_- and their movement at applied static stress $\sigma_s \propto F_s$.

energy which has to be overcome to create a domain wall, we observe that the number of twin walls $N_w \propto \exp[-\frac{(T_c-T)^{3/2}}{T}]$ will increase exponentially upon approaching T_c. But even so one does not get an equilibrium domain configuration. A loophole can be found by inspecting the real domain structure in perovskites which usually consists of needle shaped domains.[28,41] A sketch of such needle domains is shown in Fig. 2.

Such needle shaped domains are formed in ferroelastic crystals due to mechanical incompatibilities of the lattice occurring around domain wall intersections.[21] Rotational defects (wedge disclinations) located at the domain wall junctions create long range stresses, which lead to phenomena such as humping and wiggling of neighboring domain walls, the formation of needle tips, and splitting of needle tips.[21] Bornarel[3,52] has done beautiful work in KH_2PO_4, showing that domain tips produce long range interactions between domains. Torrès *et al.*[53] have shown that these long range elastic stress fields can *stabilize* an array of ferroelastic needle domains. Their free energy [Eq. (44) of Ref. 53] contains a term $\propto \epsilon_s^2 x_0$, where $x_0 = \frac{1}{2}(x_+ + x_-)$ is the average domain width. This term, which arises from the long range elastic interactions between needle shaped domains, is reminiscent of the term $\propto P_s^2 x_0$, which appears in the free energy of an array of *ferroelectric* domains[19] due to long range electrostatic forces.

Generally we have to distinguish between two types of domain boundary motion: Domain boundaries can shift "sideways" under external stress, i.e., along the normal to their domain boundaries with amplitude ξ. The second type of movement of such needles is that of retraction and progression of the needle tip with amplitude λ. However, one should also note that for long needles the lateral displacement ξ of domain walls causes a much larger change in cross-sectional area as does λ, and therefore the contribution of lateral movement to the macroscopic susceptibility may overcome the longitudinal one. Such situation was previously observed for KH_2PO_4.[52]

Now one could proceed in a similar way as for ferroelectric crystals,[9,19] resulting in a domain wall contribution to the elastic compliance $\Delta S_{11}^{\mathrm{DW}}$ of the form

$$\Delta S_{11}^{\mathrm{DW}} = \frac{\epsilon_s}{x_0}\frac{\partial \xi}{\partial \sigma}. \tag{4}$$

Torrès *et al.*[53] have calculated the average domain size x_0 for an array of needle shaped domains as

$$x_0 \propto \frac{\sqrt{E_w l}}{\epsilon_s}, \tag{5}$$

where l is the length of the needles and E_w the domain wall energy. With Eq. (4) and $\frac{\partial \xi}{\partial \sigma} = \epsilon_s/q$, where q is an effective spring constant, one obtains

$$\Delta S_{11}^{\mathrm{DW}} \propto \frac{\epsilon_s^3}{\sqrt{E_w l}}. \tag{6}$$

Since for all the measured perovskites in the improper ferroelastic phases the relation $\epsilon_s \propto Q(T)^2$ holds,[27,28,39] one obtains for a second order phase transition, with the primary order parameter $Q \propto (T_c - T)^{1/2}$ and $E_w \propto (T_c - T)^{3/2}$,

$$\Delta S_{11}^{\mathrm{DW}} \propto (T_c - T)^{9/4} \propto Q^4\sqrt{Q}. \tag{7}$$

Although Eq. (7) describes the superelastic softening qualitatively well, it fails for a quantitative fit of the data. In fact all measurements clearly show that for perovskites the domain wall contribution to the elastic response is proportional to the square of the order parameter; i.e., $\Delta S^{\mathrm{DW}} \propto Q^2$. This very robust result was found for $SrTiO_3$,[27] $KMn_{1-x}Ca_xF_3$,[28] and $LaAlO_3$.[29] It can be most clearly seen in the example of $LaAlO_3$ in Fig. 6 of Ref. 29, which displays $\Delta S^{\mathrm{DW}} \propto Q^2 \propto (T_c - T)$.

To overcome this discrepancy, we recall that most of the theories of domain wall motion effects neglect the thickness w of domain walls. However, it has been shown that ferroelastic domain walls are rather thick (e.g., $w \approx 3$ and 10 times the lattice spacing normal to the twin plane for $SrTiO_3$ and $LaAlO_3$, respectively),[54] displaying a critical temperature dependence, when approaching T_c. For example, for $LaAlO_3$ the domain wall width varies between 10 nm (300 K) and 50 nm (800 K).[54] To account for the finite width of domain walls we adapt the phenomenological Landau-Ginzburg-Lifshitz model which was previously used for the description of incommensurate-commensurate (INC-C) phase transitions[55] and originally developed for magnetic phase transitions.[56,57] Sannikov[55] mentioned the similarity of the solutions of the Euler-Lagrange equations for incommensurate systems and domain structures, due to the absence of the coefficient of the Lifshitz term in these equilibrium equations. In fact Shirobokov[58] has already calculated the effect of an external magnetic field on the magnetic domain structure of ferromagnetics by analyzing the so called Bloch-Landau-Lifshitz model.

Including the repulsion between extended domain walls[59,60] and taking into account the long range elastic interactions between needle shaped domains[53] in the free energy density f, one obtains in the presence of an applied stress σ

$$\begin{aligned} f(\sigma) = f_L &+ k\epsilon_s^2(x_+ + x_-) \\ &+ \frac{1}{x_+ + x_-}[E_w + b\exp(-x_+/w) + b\exp(-x_-/w)] \\ &+ 2\epsilon_s\sigma\frac{x_+}{x_+ + x_-}, \end{aligned} \tag{8}$$

where x_+ and x_- denote the widths of the two different domains, w is the domain wall width (Fig. 2), and the approximation works well if $x_+ \gg w$ and $x_- \gg w$. The

term $E_w > 0$ represents the domain wall energy (per unit area) and the term with b describes the repulsion ($b > 0$) between domain walls. f_L is the homogeneous part of the Landau-Ginzburg potential including order parameter strain coupling terms, which was published in a number of papers for the cubic to tetragonal[31] as well as the cubic to rhombohedral[39] transition, respectively. Equation (8) differs from the free energy density used for the description of solitons[55] of an incommensurate phase near the lock-in transition. Due to the Lifshitz term in the free energy of incommensurate phases the energy of discommensurations in the incommensurate phase near the lock-in transition is *negative*, whereas the domain wall energy E_w is *positive*. This leads to a stable soliton lattice sufficiently near the lock-in transition with an equilibrium distance between discommensurations, which is strongly temperature dependent. One of the most interesting consequences from this is the well known Curie-Weiss type anomaly of the dielectric susceptibility[61] or the elastic susceptibility[36] when approaching the improper ferroelectric or ferroelastic lock-in transition, respectively. In contrast to this, due to the positive domain wall energy contribution, ferroelastic domains are generally metastable objects. However, the long range elastic interactions between needle shaped domains, which in Eq. (8) enter through the term $k\epsilon_s^2(x_+ + x_-)$, stabilize a ferroelastic domain structure in the present case. It turns out that Eq. (8) is very useful for the description of the observed superelastic softening in perovskites and one can proceed as follows. Under applied stress $\sigma = \sigma_s + \delta\sigma$ (σ_s and $\delta\sigma$ static and dynamic components of stress, respectively) the width x_+ of domains with $\epsilon_s(+)$ enlarges, while the width x_- of domains with $\epsilon_s(-)$ shrinks (Fig. 2). This leads to a new period $x_0(\sigma) = x_+(\sigma) + x_-(\sigma)$ of the domain lattice under applied stress. The macroscopic deformation ϵ^{DW} of the crystal due to domain wall motion under applied stress is

$$\epsilon^{\mathrm{DW}} = \epsilon_s \frac{x_+ - x_-}{x_+ + x_-} = \epsilon_s \left(1 - \frac{x_-}{x_0}\right). \tag{9}$$

Assuming that x_0 is a function of the static stress σ_s only and does not depend on the oscillating part, i.e., the so called clamped compliance condition[60] $(\partial x_+/\partial\sigma)_{x_0} = -(\partial x_-/\partial\sigma)_{x_0}$, one obtains the domain wall contribution to the elastic compliance:

$$\Delta S^{\mathrm{DW}} = -\frac{\epsilon_s}{x_0}\left(\frac{\partial x_-}{\partial\sigma}\right)_{x_0}. \tag{10}$$

The equilibrium conditions $\partial f(\sigma)/\partial x_\pm = 0$ lead with Eq. (8) to the following two transcendental equations:

$$\begin{aligned} &k\epsilon_s^2 - \frac{1}{4x_0^2}[E_w + b\exp(-x_+/w) + b\exp(-x_-/w)] \\ &\quad - \frac{b}{2wx_0}\exp(-x_+/w) + \frac{\epsilon_s\sigma}{x_0} - \frac{\epsilon_s\sigma x_+}{2x_0^2} = 0, \\ &k\epsilon_s^2 - \frac{1}{4x_0^2}[E_w + b\exp(-x_+/w) + b\exp(-x_-/w)] \\ &\quad - \frac{b}{2wx_0}\exp(-x_-/w) - \frac{\epsilon_s\sigma x_+}{2x_0^2} = 0. \end{aligned} \tag{11}$$

Combining both equilibrium conditions yields

$$\exp(-x_-/w) - \exp(-x_+/w) = \frac{2\sigma\epsilon_s w}{b}. \tag{12}$$

Using Eq. (12) and the clamped compliance condition we obtain $\partial x_-/\partial\sigma = -\frac{2\epsilon_s w^2}{b\exp(-x_-/w)+b\exp(-x_+/w)}$ which together with Eq. (10) leads to

$$\Delta S^{\mathrm{DW}} = \frac{2\epsilon_s^2 w^2}{bx_0(\sigma)[\exp(-x_-(\sigma)/w) + \exp(-x_+(\sigma)/w)]}. \tag{13}$$

At this point Eq. (13) is identical to the form of the elastic compliance near the lock-in transition to an improper ferroelastic INC-C lock-in phase [see Eq. (19) of Ref. 36]. The difference to our case however comes from the different temperature dependence of the domain width x_0 as compared to the width of the soliton lattice. For vanishing applied static stress $\sigma_s \to 0$ the condition $x_- = x_+ = x_0$ holds and

$$\Delta S^{\mathrm{DW}} = \frac{\epsilon_s^2 w^2}{bx_0\exp(-x_0/w)}. \tag{14}$$

For further evaluation we calculate the equilibrium domain width x_0 from Eq. (11) at $\sigma = 0$ according to

$$x_0^2 4k\epsilon_s^2 - 2b\exp(-x_0/w)\left[1 + \frac{x_0}{w}\right] - E_w = 0. \tag{15}$$

For the general case the transcendental equation (15) can only be solved numerically. Before doing this, it is instructive to look first at the solution neglecting the repulsion between domain walls, as has been done by Tórres *et al.*,[53] yielding

$$x_0 = \frac{\sqrt{E_w}}{2\sqrt{k}\epsilon_s}. \tag{16}$$

Although the repulsion term between domain walls is neglected here, this relation may be used for a qualitative understanding of the differences in the temperature evolution observed in various ferroelastic materials. For example in the proper ferroelastic phase of NdP_5O_{14} a regular striped pattern was observed, where the number N_w of domains increases drastically with approaching T_c from below.[20,62] In contrast for $KMnF_3$,[63] $SrTiO_3$,[64] and $LaAlO_3$[65] no such strong variation of the domain wall density is observed in their whole improper ferroelastic phase (see also Fig. 3). Since for a proper ferroelastic crystal the spontaneous strain is the primary order parameter[21] varying close to a second order phase transition as $\epsilon_s \propto (T_c - T)^{1/2}$ and $E_w \propto (T_c - T)^{3/2}$, according to Eq. (16) the number of twin walls $N_w \propto 1/x_0 \propto (T_c - T)^{-1/4}$ is increasing with increasing temperature, i.e., is diverging at T_c. In contrast, for an improper ferroelastic phase transition the spontaneous strain is proportional to the square of the order parameter and thus varies as $\epsilon_s \propto Q^2 \propto (T_c - T)$. Inserting this into Eq. (16) leads to $N_w \propto 1/x_0 \propto (T_c - T)^{+1/4}$. This opposite temperature dependence of the number of domain walls or equivalently the average domain width for proper and improper ferroelastic crystals may well explain the different observed temperature evolutions of ferroelastic domains.

Now let us return to describe the elastic measurements on perovskites. As already mentioned above, x_0 cannot be calculated analytically, but a numerical solution of Eq. (15)

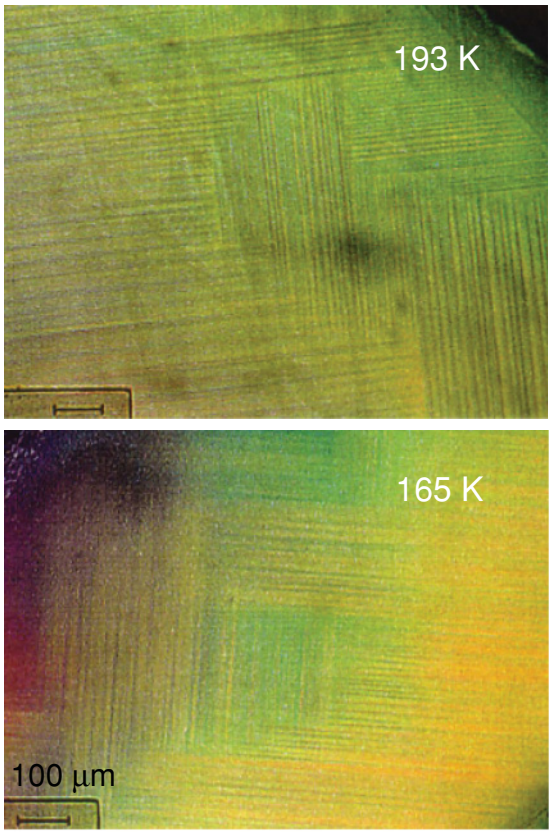

FIG. 3. (Color online) Needle-shaped ferroelastic domains in $KMn_{0.983}Ca_{0.017}F_3$ at $T = 193$ K and 165 K observed with polarizing microscope.

shows that one can find a reasonable set of parameters where $x_0 \exp(-x_0/w)$ is almost independent of temperature, except for a very small temperature range close to T_c (Fig. 4). (Note that for INC-C transitions $x_0 \exp(-x_0/w) = wE_w$, i.e., is strongly temperature dependent, which is the origin for the Curie-Weiss type anomaly in the susceptibility close to the lock-in transition [see, e.g., Eq. (25b) of Ref. 59].) Therefore the temperature dependence of ΔS^{DW} in Eq. (14) is determined by the temperature dependencies of $\epsilon_s \propto Q^2(T)$ and the square of the domain wall width $w(T)$, which was shown[21] to vary as $w^2 = \frac{2g}{BQ^2+2CQ^4}$, where B and C are the fourth and sixth order expansion coefficients of the Landau free energy and g is the coefficient of the gradient term. Inserting these relations into Eq. (14), we obtain

$$\Delta S^{\mathrm{DW}} \propto \frac{Q^4}{BQ^2\left(1+\frac{2C}{B}Q^2\right)}. \tag{17}$$

The Landau expansion coefficients for the present perovskites have been previously determined[35,54] with great accuracy and are collected in Table I. For $LaAlO_3$ the agreement of the present model with the experimental data can be most easily demonstrated. Since the phase transition in $LaAlO_3$ is continuous and well described by a 2-4 Landau expansion, i.e., with $C = 0$ (Table I), according to Eq. (17) $\Delta S^{\mathrm{DW}} \propto Q^2 \propto (T_c - T)$ (inset of Fig. 4), which is in perfect

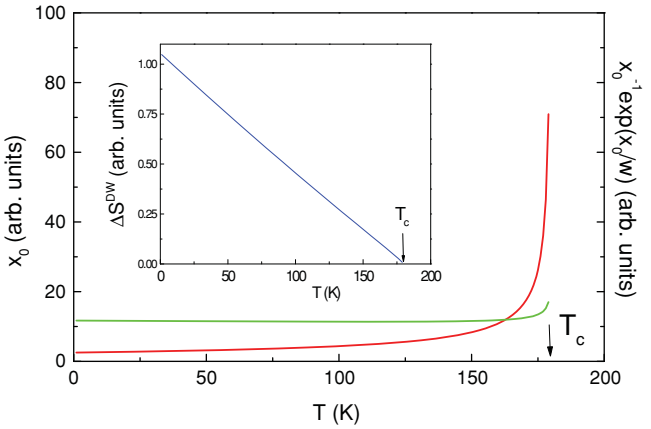

FIG. 4. (Color online) Temperature dependencies of x_0 (red line), $x_0^{-1}e^{x_0/w}$ (green line), and ΔS^{DW} (blue line of inset) calculated from Eq. (15) for a second order phase transition.

agreement with the experimental data (Fig. 6 of Ref. 29). For $SrTiO_3$ it has been shown[24,35] that

$$Q^2 = -\frac{B}{2C} + \sqrt{\left(\frac{B}{2C}\right)^2 - \frac{A\theta_s}{C}\left[\coth\left(\frac{\theta_s}{T}\right) - \coth\left(\frac{\theta_s}{T_c}\right)\right]}, \tag{18}$$

with $\theta_s = 60.75$ K and A, B, and C from Table I, whereas for pure and mixed fluoroperovskites the classical order parameter solution of the 2-4-6 Landau expansion is used.[35] We have fitted our experimental data according to equation $Y^r = (1 + \Delta S^{\mathrm{DW}} + \Delta S^{\mathrm{LK}})^{-1}$, where ΔS^{DW} and ΔS^{LK} are the domain wall and the Landau-Khalatnikov (LK) contributions, respectively. The LK contributions for $SrTiO_3$[27,31] as well as for $KMnF_3$[28] have been determined previously and it was shown that they are very small (<10%) compared to the domain wall contribution (up to about 80%). Figures 5 and 6 show that the data for $\sigma_s = 0$ can be perfectly fitted with Eqs. (17) and (18) and the parameters of Table I.

To describe the stress dependence of ΔS^{DW} we have to calculate $x_0(\sigma_s)$ from Eq. (11). Again this cannot be solved analytically, but we can perform a rough approximation. For increasing stress, x_+ increases and x_- decreases which according to Eq. (12) saturates at

$$\exp(-x_-/w) = \frac{2\sigma\epsilon_s w}{b}, \tag{19}$$

TABLE I. Landau coefficients for the $Pm\bar{3}m$–$I4/mcm$ phase transition of some perovskites.

	A (J/mol K)	B (J/mol)	C (J/mol)
$KMnF_3$	2.72	−57.38	573
$KMnF_3$ 1.7% Ca	2.87	20	540
$SrTiO_3$	0.7	31.22	42.2
$LaAlO_3$	4.49	3670	0

whereas $\exp(-x_+/w) \to 0$ for $\sigma \to \infty$. Inserting this into Eq. (13) we obtain

$$\Delta S^{\mathrm{DW}} = \frac{\epsilon_s^2 w^2}{b x_0(\sigma)\left[\exp(-x_+(\sigma)/w) + \frac{\sigma \epsilon_s w}{b}\right]}. \quad (20)$$

In the same limit of high stress we obtain for the average domain size

$$x_0(\sigma) = \sqrt{\frac{E_w + 2\sigma\epsilon_s w\left[1 - \ln\left(\frac{2\sigma\epsilon_s w}{b}\right)\right]}{4k\epsilon_s^2}}. \quad (21)$$

Inserting x_0 into Eq. (20) we get

$$\Delta S^{\mathrm{DW}} = \frac{\epsilon_s^2 w^2}{\sqrt{\frac{E_w + 2\sigma\epsilon_s w\left[1 - \ln\left(\frac{2\sigma\epsilon_s w}{b}\right)\right]}{4k\epsilon_s^2}}\left[e^{-x_+(\sigma)/w} + \frac{\sigma\epsilon_s w}{b}\right]}. \quad (22)$$

Figure 5 shows that the present model fits the data for $SrTiO_3$ perfectly in the whole measured temperature and stress range. For $KMn_{0.983}Ca_{0.017}F_3$, however, the agreement is not so good. The inset of Fig. 6 shows a fit of the data using Eq. (22). Although the data are well described for small applied static load (stress), the fits worsen with increasing load (stress). The origin of this difference with $SrTiO_3$ is presently not clear. One possibility is that the strong nonlinearity of ΔS^{DW} with respect to σ_s is due to a strong suppression of the number of domain walls as has been described by a coarse-grained Ising type model with spin-strain coupling.[20,28] It may however also be described in the frame of the present continuum model, if we take into account that even a very small applied stress leads in $KMnF_3$ to a retraction of the needle shaped domains as we have observed in polarizing microscopy under applied stress. In a very simplified model we can calculate the effect of needle retraction to the elastic susceptibility by multiplying ΔS^{DW} of Eq. (22) with $l_-(\sigma)$. Since in first approximation $l_- \propto 1/\sigma$, this increases the nonlinearity of ΔS^{DW} with respect to σ, which leads to a much better agreement with the data (Fig. 6).

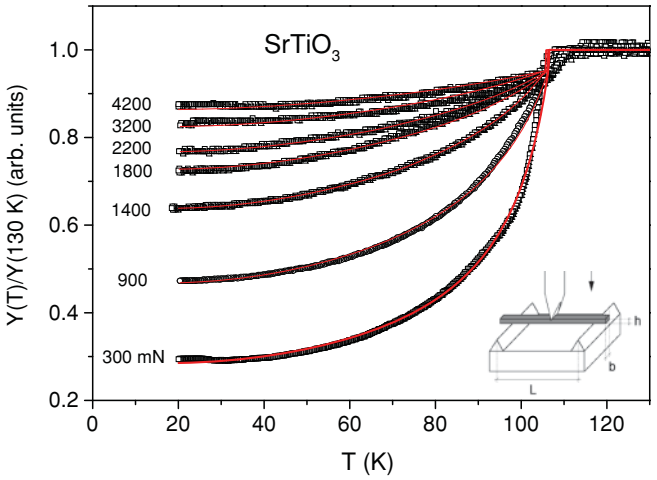

FIG. 5. (Color online) Temperature dependence of the relative Young's modulus of $SrTiO_3$ crystals measured by the three point bending method with different static loads $F_s \propto \sigma_s$ at $f = 11$ Hz. Sample size: $6.7 \times 1.5 \times 0.44$ mm^3. The lines are the fits using Eq. (22) and $Y^r = (1 + \Delta S^{\mathrm{DW}} + \Delta S^{\mathrm{LK}})^{-1}$.

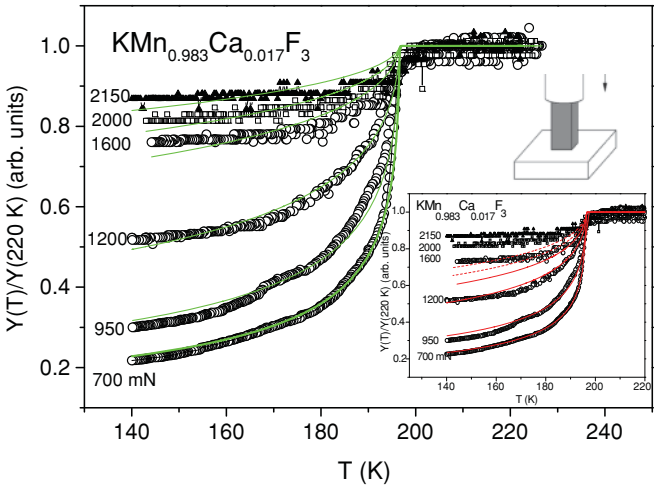

FIG. 6. (Color online) Temperature dependence of the relative Young's modulus of $KMn_{0.983}Ca_{0.017}F_3$ crystals measured by the parallel plate method with different static loads $F_s \propto \sigma_s$ at $f = 13$ Hz. Sample size: $1 \times 1 \times 3$ mm^3. The lines are fits with Eq. (22) and $Y^r = (1 + \Delta S^{\mathrm{DW}} + \Delta S^{\mathrm{LK}})^{-1}$, assuming an additional stress dependence of the length of needle shaped domains as described in the text. Inset: Fit with Eq. (22) assuming constant length of the needles.

V. SUMMARY

We have performed a detailed analysis of the "superelastic softening" measured recently by dynamic mechanical analysis in quite a number of various perovskite structured materials including $SrTiO_3$,[26,27] $Ca_{1-x}Sr_xTiO_3$,[66] $LaAlO_3$,[40,41] $KMnF_3$, $KMn_{1-x}Ca_xMnF_3$,[28] and $BaCeO_3$.[67] This pronounced softening, which is observed in the improper ferroelastic phases of the crystals at low measurement frequencies (0.1–50 Hz) originates from the movement of thousands of ferroelastic twin boundaries in response to the externally applied dynamic stress. To calculate the domain wall motion induced contribution to the elastic susceptibility ΔS^{DW} we first had to overcome the stability problem of ferroelastic domains. This was done by considering the real domain structure of perovskites. Practically in all the measured crystals the domains in the ferroelastic phases form needle shapes. The tips of these needles produce long range stresses[3,52] which lead to long range interactions between domain walls[53] that are formally identical to the long range interactions in ferroelectric or ferromagnetic systems and are therefore in a similar way stabilizing an array of ferroelastic domains. The corresponding free energy can be used to calculate the average domain width x_0 and the effective "spring constant" of the domain array, which yields an elastic softening with a magnitude proportional to the square of the spontaneous strain, i.e., $\Delta S^{\mathrm{DW}} \propto \frac{\epsilon_s^2}{x_0}$, which is again formally identical to the domain wall contribution to the dielectric susceptibility of ferroelectrics.[19] Since for the improper ferroelastic perovskites the spontaneous strain itself is proportional to the square of the order parameter, $\Delta S^{\mathrm{DW}} \propto Q(T)^4$ would hold. But this result is in contradiction to the fact that all measured perovskite crystals yield a domain wall contribution $\Delta S^{\mathrm{DW}} \propto Q(T)^2$. Up to this point all calculations were performed with the assumption of infinitely thin domain walls. However, it was impressively

shown[54] that ferroelastic domain walls have a finite thickness w which increases as $w \propto 1/Q(T)$ when approaching T_c. Taking into account the repulsion between domain walls of finite width w, the elastic susceptibility is multiplied by $w^2 \propto 1/Q^2$, leading to $\Delta S^{\mathrm{DW}} \propto \frac{\epsilon_s^2 w^2}{x_0} \propto Q(T)^2$, which then perfectly fits the data for small applied stress. For higher external stresses, the width of ferroelastic domains decreases, leading to a nonlinear stress dependence of the domain wall contribution to the elastic compliance. At very high stress the whole crystal is switched to a (nearly) single-domain state and the elastic compliance approaches the monodomain value, which is determined by the Landau-Khalatnikov (LK) contribution ΔS^{LK}.

At ultrasonic frequencies ($f = 15$ MHz) the domain walls can no longer follow the stress field and the superelastic softening vanishes. The remaining elastic anomalies can then be well fitted within Landau theory taking into account the coupling terms between the order parameter and the strain components (LK contribution).

We can conclude that for understanding of the domain wall contributions of ferroic materials to the corresponding macroscopic susceptibilities the effect of domain wall thickness and its critical temperature dependence have to be taken into account. The present results may also serve as a basis for further investigations of domain or nanodomain induced effects in other materials, e.g., with proper ferroelastic phase transitions, martensitic phase transitions, or even strain glasses.

ACKNOWLEDGMENTS

The author thanks A. Tröster and M. Fally for many stimulating discussions and valuable comments. The present work was supported by Austrian FWF Project No. P19284-N20.

*wilfried.schranz@univie.ac.at

[1] G. Busch and P. Scherrer, Naturwissenschaften **23**, 737 (1935).
[2] E. A. Little, Phys. Rev. **4**, 978 (1955).
[3] J. Bornarel, J. Appl. Phys. **43**, 845 (1972).
[4] K. Kuramoto, J. Phys. Soc. Jpn. **56**, 1859 (1987).
[5] Y. N. Huang, Y. N. Wang, and H. M. Shen, Phys. Rev. B **46**, 3290 (1992).
[6] V. Mueller, Y. Shchur, H. Beige, A. Fuith, and S. Stepanow, Europhys. Lett. **57**, 107 (2002).
[7] M. Fally, P. Kubinec, A. Fuith, W. Schranz, C. Filipic, and H. Warhanek, Ferroelectrics **172**, 157 (1995).
[8] Y. N. Huang, X. Li, Y. Ding, Y. N. Wang, H. M. Shen, Z. F. Zhang, C. S. Fang, S. H. Zhuo, and P. C. W. Fung, Phys. Rev. B **55**, 16159 (1997).
[9] N. A. Pertsev and G. Arlt, J. Appl. Phys. **74**, 4105 (1993).
[10] W. Kleemann, Annu. Rev. Mater. Res. **37**, 415 (2007).
[11] Y. Wang, X. Ren, and K. Otsuka, Mater. Sci. Forum **583**, 67 (2008).
[12] A. K. Tagantsev, L. E. Cross, and J. Fousek, *Domains in Ferroic Crystals and Thin Films* (Springer, Berlin, 2010).
[13] V. K. Wadhawan, *Introduction to Ferroic Materials* (Gordon and Breach Science Publishers, Amsterdam, 2010).
[14] C. Kittel, Phys. Rev. **83**, 458 (1951).
[15] G. Arlt and N. A. Pertsev, J. Appl. Phys. **70**, 2283 (1991).
[16] A. S. Sidorkin, J. Appl. Phys. **83**, 3762 (1998).
[17] Ó. Alejos, C. de Francisco, J. M. Muñoz, P. Hernández, and C. Torres, Phys. Rev. B **58**, 8640 (1998).
[18] T. Nattermann, V. Pokrovsky, and V. M. Vinokur, Phys. Rev. Lett. **87**, 197005 (2001).
[19] A. S. Sonin and B. A. Strukov, *Introduction to Ferroelectricity* [in Russian] (Moscow, 1970).
[20] X. R. Huang, S. S. Jiang, X. B. Hu, X. Y. Xu, W. Zeng, D. Feng, and J. Y. Wang, Phys. Rev. B **52**, 9932 (1995).
[21] E. K. H. Salje, *Phase Transitions in Ferroelastic and Co-elastic Crystals* (Cambridge University Press, Cambridge, 1990).
[22] J. Sapriel, Phys. Rev. B **12**, 5128 (1975).
[23] E. K. H. Salje and Y. Ishibashi, J. Phys. Condens. Matter **8**, 8477 (1996).
[24] E. K. H. Salje, A. Buckley, G. van Tendeloo, Y. Ishibashi and G. L. Nord Jr., Am. Mineral. **83**, 811 (1998).
[25] W. Schranz and I. Rychetsky, J. Phys. Condens. Matter **5**, 3871 (1993).
[26] A. V. Kityk, W. Schranz, P. Sondergeld, D. Havlik, E. K. H. Salje, and J. F. Scott, Europhys. Lett. **50**, 41 (2000).
[27] A. V. Kityk, W. Schranz, P. Sondergeld, D. Havlik, E. K. H. Salje, and J. F. Scott, Phys. Rev. B **61**, 946 (2000).
[28] W. Schranz, P. Sondergeld, A. V. Kityk, and E. K. H. Salje, Phys. Rev. B **80**, 094110 (2009).
[29] R. J. Harrison and S. A. T. Redfern, Phys. Earth Planet. Interiors **134**, 253 (2002).
[30] S. Geller and V. B. Bala, Acta Cryst. **9**, 1019 (1956).
[31] J. C. Slonczewski and H. Thomas, Phys. Rev. B **1**, 3599 (1970).
[32] E. K. H. Salje, M. C. Gallardo, J. Jiménez, F. J. Romero, and J. del Cerro, J. Phys. Condens. Matter **10**, 5535 (1998).
[33] S. Bueble, K. Knorr, E. Brecht, and W. W. Schmahl, Surf. Sci. **400**, 345 (1998).
[34] F. J. Romero, M. C. Gallardo, S. A. Hayward, J. Jimnez, J. del Cerro, and E. K. H. Salje, J. Phys. Condens. Matter **16**, 2879 (2004).
[35] M. C. Gallardo, F. J. Romero, S. A. Hayward, E. K. H. Salje, and J. D. Cerro, Mineral. Mag. **64**, 971 (2000).
[36] A. V. Kityk, V. P. Soprunyuk, A. Fuith, W. Schranz, and H. Warhanek, Phys. Rev. B **53**, 6337 (1996).
[37] W. Schranz, Phase Transitions **64**, 103 (1997).
[38] P. Sondergeld, W. Schranz, A. Tröster, M. A. Carpenter, E. Libowitzky, and A. V. Kityk, Phys. Rev. B **62**, 6143 (2000).
[39] M. A. Carpenter, S. V. Sinogeikin, and J. D. Bass, J. Phys. Condens. Matter **22**, 035404 (2010).
[40] R. J. Harrison, S. A. T. Redfern, and E. K. H. Salje, Phys. Rev. B **69**, 144101 (2004).
[41] R. J. Harrison, S. A. T. Redfern, A. Buckley, and E. K. H. Salje, J. Appl. Phys. **95**, 1706 (2004).
[42] C. Wang, S. A. T. Redfern, M. Daraktchiev, and R. J. Harrison, Appl. Phys. Lett. **89**, 152906 (2006).
[43] Y. N. Wang, Y. N. Huang, H. M. Shen, and Z. F. Zhang, J. Physique IV, Colloq. **6**, C8–505 (1996).
[44] Th. Braun, W. Kleemann, J. Dec, and P. A. Thomas, Phys. Rev. Lett. **94**, 117601 (2005).

[45] J. Hlinka, P. Ondrejkovic, and P. Marton, Nanotechnol. **20**, 105709 (2009).
[46] V. K. Wadhawan, Phase Transitions **3**, 3 (1982).
[47] M. Liu, T. R. Finlayson, and T. F. Smith, Phys. Rev. B **55**, 3480 (1997).
[48] A. Gibaud, S. M. Shapiro, J. Nouet, and H. You, Phys. Rev. B **44**, 2437 (1991).
[49] S. A. Hayward, S. A. T. Redfern, and E. K. H. Salje, J. Phys. Condens. Matter **14**, 10131 (2002).
[50] A. L. Roytburd, J. Appl. Phys. **83**, 228 (1998).
[51] A. L. Roytburd, J. Appl. Phys. **83**, 239 (1998).
[52] J. Bornarel and J. Lajzerowicz, J. Appl. Phys. **39**, 4339 (1968).
[53] J. Torrès, C. Roucau, and R. Ayroles, Phys. Status Solidi (a) **70**, 193 (1982).
[54] J. Chrosch and E. K. H. Salje, J. Appl. Phys. **85**, 722 (1999).
[55] D. G. Sannikov, in *Incommensurate Phases in Dielectrics*, Vol. 1, *Fundamentals*, ed. R. Blinc and A. P. Levanyuk (North-Holland Physics Publishing, Amsterdam, 1986).
[56] I. E. Dzyaloshinskii, Sov. Phys. JETP **19**, 960 (1964).
[57] I. E. Dzyaloshinskii, Sov. Phys. JETP **20**, 665 (1965).
[58] Y. A. Shirobokov, Zh. Eksp. Teor. Fiz. **15**, 57 (1945).
[59] P. Prelovsek, J. Phys. C **16**, 3257 (1983).
[60] J. Holakovsky and V. Dvorak, J. Phys. C **21**, 5449 (1988).
[61] A. Levstik, P. Prelovsek, C. Filipic, and B. Zeks, Phys. Rev. B **25**, 3416 (1982).
[62] W. Yaning, S. Wenyuan, C. Xiaohua, S. Humin, and L. Baosheng, Phys. Status Solidi A **102**, 279 (1987).
[63] A. Okazaki, Y. Soejma, and M. Machida, J. Phys. C **20**, 1041 (1987).
[64] L. Cao, E. Sozontov, and J. Zegenhagen, Phys. Status Solidi A **181**, 387 (2000).
[65] S. A. Hayward, F. D. Morrison, S. A. T. Redfern, E. K. H. Salje, J. F. Scott, K. S. Knight, S. Tarantino, A. M. Glazer, V. Shuvaeva, P. Daniel, M. Zhang, and M. A. Carpenter, Phys. Rev. B **72**, 054110 (2005).
[66] R. J. Harrison, S. A. T. Redfern, and J. Street, Am. Mineral. **88**, 574 (2003).
[67] Z. Zhang, J. Koppensteiner, W. Schranz, J. B. Betts, A. Migliori, and M. A. Carpenter, Phys. Rev. B **82**, 014113 (2010).